DEUTSCHES ELEKTRONEN – SYNCHROTRON
INSTITUT FÜR HOCHENERGIEPHYSIK

DESY 92-038
March 1992

Structure Functions and QCD Tests at HERA

J. Blümlein, M. Klein

Deutsches Elektronen-Synchrotron DESY
Institut für Hochenergiephysik IfH, Zeuthen

ISSN 0418-9833

PLATANENALLEE 6 · O-1615 ZEUTHEN

To be sure that your preprints are promptly included in the
HIGH ENERGY PHYSICS INDEX,
send them to the following (if possible by air mail):

DESY Bibliothek Notkestraße 85 W-2000 Hamburg 52 Germany	DESY-IfH Bibliothek Platanenallee 6 O-1615 Zeuthen Germany

DESY 92-038
March 1992

ISSN 0418-9833

Structure Functions and QCD Tests at HERA

J.Blümlein and M.Klein
DESY-Institut für Hochenergiephysik, Zeuthen, Germany

Abstract

A study is presented on the possibilities to measure the neutral and charged current structure functions F_2, xG_3 and W_2 for electron-proton and electron-deuteron deep inelastic scattering at HERA. A QCD analysis is performed for a combination of neutral current cross sections and simulated data sets at different c.m.s. energies.

1 Introduction

With the advent of the *ep* collider HERA the kinematical range in which nucleon structure functions are measured will be extended in a twofold way: *i)* to *high* $Q^2 \sim 10^4$ GeV^2 for $x \sim 0.5$ and *ii)* to *small* $x \sim 10^{-4}$ for $Q^2 \sim 10$ GeV^2. Compared to the 1987 Workshop the main result of this Study Group has been that the accessible (Q^2, x) range can be larger than previously estimated if, in certain regions, the electron and the hadronic Q^2 and x measurements are combined [1, 2] and use is made of 'mixed' variables, e.g. Q^2 measured at the leptonic vertex and y at the hadronic vertex. Different kinematical conditions will be discussed in the analysis in order to: *i)* isolate various structure functions from cross section measurements (e.g. F_L and F_2), *ii)* measure the neutral current cross section continuously from the region probed by fixed target experiments so far up to highest values of Q^2 and *iii)* determine Λ in different ranges of x, which corresponds to the measurement of $\alpha_s(Q^2)$ at different values of Q^2.

Subsequently we present a brief update of our earlier studies [3, 4] based on the extended kinematic range. In particular, we investigate the prospects to measure the structure functions $F_2(x, Q^2)$, $xG_3(x, Q^2)$ and $W_2(x, Q^2)$ in neutral current deep inelastic *ep* and *ed* scattering (section 2) and to test perturbative QCD *via* the Q^2 evolution of F_2 (section 3). Our conclusions are presented in section 4.

2 Structure Function Measurements

2.1 $F_2(x, Q^2)$

The deep inelastic scattering cross section of neutral current reactions $e^\pm p \to e^\pm X$ is given by

$$\frac{d^2\sigma^\pm}{dxdQ^2} = \frac{d^2\sigma_0^\pm}{dxdQ^2} + \frac{\alpha}{2\pi}\frac{d^2\sigma_1^\pm}{dxdQ^2} + \mathcal{O}(\alpha^2) \qquad (1)$$

Here, $d^2\sigma_0^\pm/dxdQ^2$ denotes the Born cross section and the other terms are the electroweak radiative corrections in first and higher order [5]. The Born cross sections are given by

$$\frac{d^2\sigma_0^\pm}{dxdQ^2} = \frac{2\pi\alpha^2}{xQ^4}\left\{Y_+\mathcal{F}_2^\pm(x,Q^2) + Y_- x\mathcal{F}_3^\pm(x,Q^2)\right\} \qquad (2)$$

with $Y_+ = 1 + (1-y)^2$, $Y_- = 1 - (1-y)^2$ for $R = 0$. The functions $\mathcal{F}_{2,3}(x, Q^2)$ represent five genuine structure functions:

$$\begin{aligned} \mathcal{F}_2^\pm(x,Q^2) &= F_2 + \kappa_Z(Q^2)(-v \mp \lambda a)G_2 + \kappa_Z^2(Q^2)(v^2 + a^2 \pm 2\lambda av)H_2 \\ x\mathcal{F}_3^\pm(x,Q^2) &= \kappa_Z(Q^2)(\pm a + \lambda v)xG_3 + \kappa_Z^2(Q^2)(-\lambda(a^2+v^2) \mp 2va)xH_3 \end{aligned} \qquad (3)$$

In the parton model one may relate these structure functions to the parton distributions by

$$\begin{aligned} [F_2, G_2, H_2] &= x\sum_q \left[e_q^2, 2e_q v_q, v_q^2 + a_q^2\right]\left[q(x,Q^2) + \bar{q}(x,Q^2)\right] \\ [xG_3, xH_3] &= 2x\sum_q [e_q a_q, v_q a_q]\left[q(x,Q^2) - \bar{q}(x,Q^2)\right] \end{aligned} \qquad (4)$$

Here v and a are the vector and axial couplings of the electron and λ denotes the lepton beam polarization. The function $\kappa_Z(Q^2) = Q^2/(Q^2 + M_Z^2)/(4\sin^2\theta_W\cos^2\theta_W)$ determines the relative strength of the contributions due to Z exchange, κ_Z, being equal to 1 at $Q^2 \sim 21.000$ GeV^2. Therefore, in most of the HERA range the neutral current cross section σ_0 is determined by the well known structure function $F_2(x, Q^2)$. Other structure functions contribute only in specific regions as high y (F_L, xG_3) and/or large Q^2 (xG_3, H_2). It is instructive to rewrite eq. 3 for unpolarized electrons ($\lambda = 0$) [1] setting $v = 0$ which is almost correct due to $\sin^2\theta = 0.230$. This leaves only a few terms from eq.3, namely

$$\begin{aligned} \mathcal{F}_2^\pm(x,Q^2) &= F_2(x,Q^2) + \kappa_Z^2(Q^2)a^2H_2(x,Q^2) \\ x\mathcal{F}_3^\pm(x,Q^2) &= \pm\kappa_Z(Q^2)axG_3(x,Q^2) \end{aligned} \qquad (5)$$

Note that the charge dependence has simplified: $\mathcal{F}_2$ becomes independent of the beam charge whereas $x\mathcal{F}_3$ changes the sign under charge conjugation.

In figure 1 the statistical precision of a measurement of the structure function $F_2(x, Q^2)$ is illustrated for the kinematical range accessible [2] at low and high energies for a luminosity of 100 pb^{-1}. Here, the KMRS parametrization B^0 was used [7] assuming a flat behaviour of the momentum distribution of the gluon at fixed Q_0^2 as $x \to 0$. The dark points will be measurable with the secondary electron only ($y \geq 0.1$). Smaller Q^2 values at fixed x, however, will be reached only using the hadronic Q^2, x measurement or even a combination of $Q^2(e)$ and $y(jet)$ giving $x = Q^2/sy$. The data sets will be overlapping which will be useful for systematic evaluations. In the region above $y \geq 0.1$ and $Q^2 \geq 50 - 100$ GeV^2, where both the electron and the jet measurement will be sufficiently precise, the comparison of both cross sections may be useful to detect large systematic effects, as miscalibrations of the calorimeter energy scales [8].

[1] As has been noticed earlier [6], small but nonzero polarization values are advantageous for simplifying the cross section formulae: a value of $\lambda(e^\pm) = \mp v/a \approx \pm 0.08$ eliminates the xG_2 term from $\mathcal{F}_2$ whereas the choice $\lambda(e^\pm) = \mp 2va/(a^2+v^2) \approx \pm 0.16$ takes off the xH_3 contribution to $x\mathcal{F}_3$.

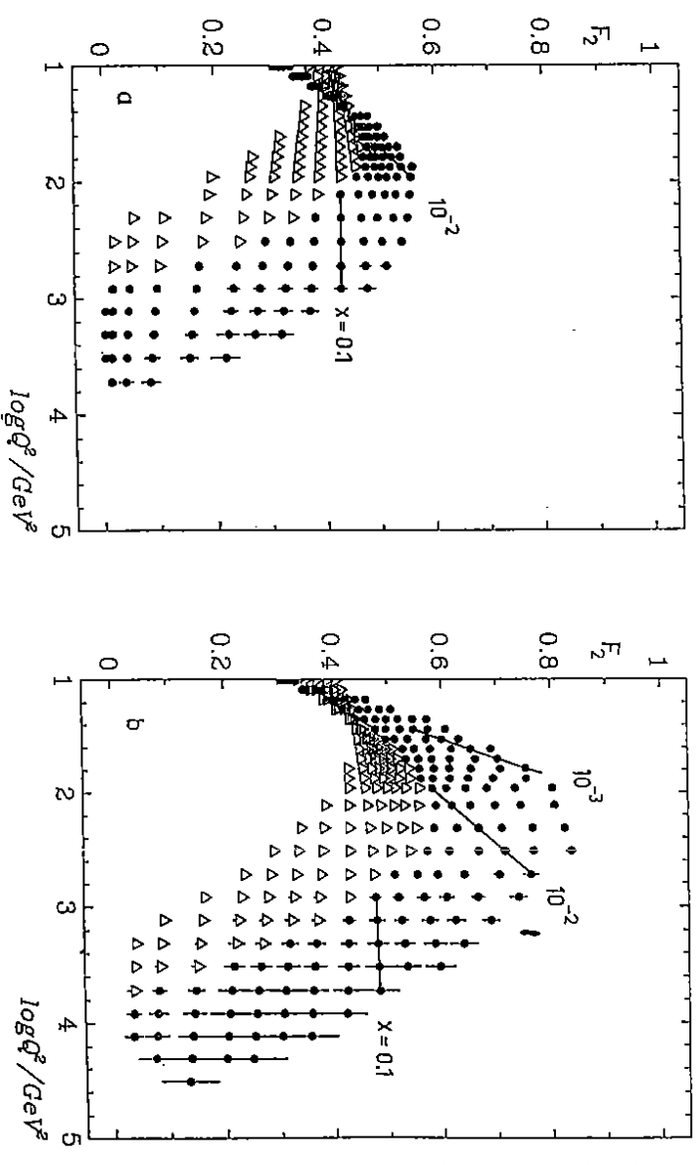

Figure 1: Expected HERA measurement of $F_2(x, Q^2)$ for a luminosity of 100 pb^{-1} at 10 × 300 (a) and 30 × 820 GeV^2 (b) in the region where one should be able to control the systematics at the required level of accuracy [2]. Only statistical errors are shown. The solid points are obtainable with electron detection only ($y \geq 0.1$). The data where simulated using the parametrization B^0 of KMRS. The x values above $x = 0.1$ are 0.14, 0.18, 0.22, 0.27, 0.35, 0.45, 0.55, 0.65. Below they are (0.16, 0.24, 0.34, 0.5, 0.7) $\cdot 10^{-n}, n = 1, 2, 3, 4$.

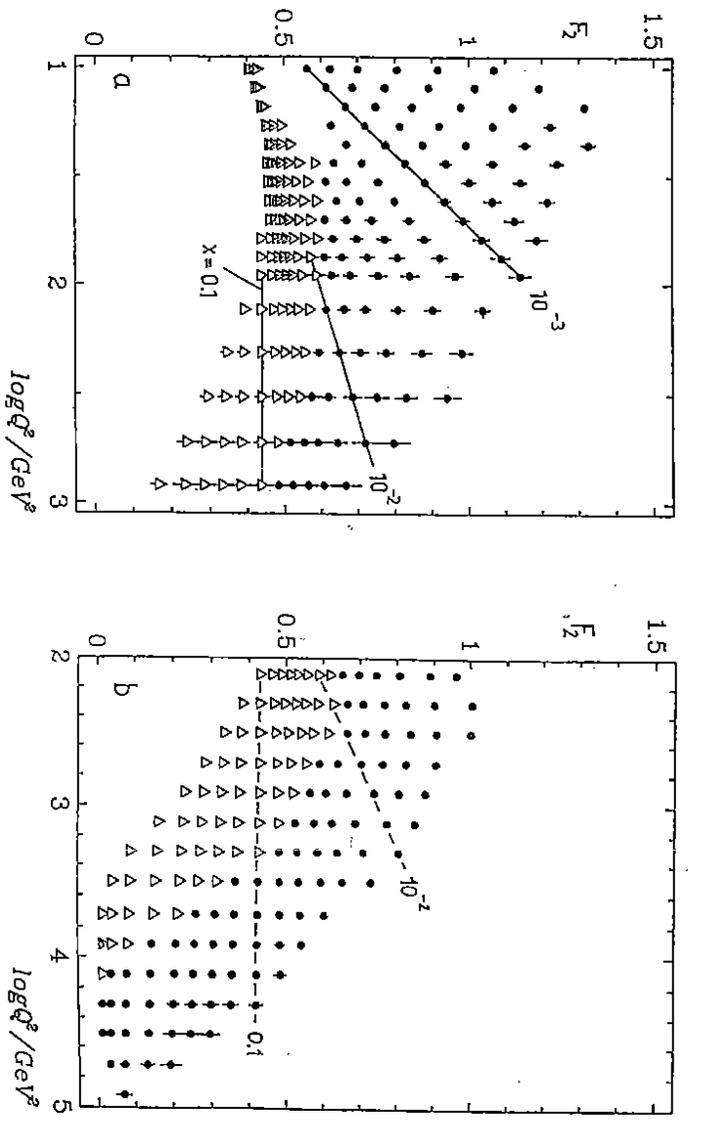

Figure 2: Expected HERA measurement of $F_2(x, Q^2)$ at lower Q^2 for a luminosity of 10 pb^{-1} at 10 × 300 (a) and at higher Q^2 for 1000 pb^{-1} at 45 × 1140 GeV^2 (b). Only statistical errors are shown. The solid points are obtainable with electron detection only ($y \geq 0.1$). The HERA data where simulated using the parametrization B^- of KMRS. The x values above $x = 0.1$ are 0.14, 0.18, 0.22, 0.27, 0.35, 0.45, 0.55, 0.65. Below they are $(0.16, 0.24, 0.34, 0.5, 0.7) \cdot 10^{-n}, n = 1, 2, 3, 4$.

As can be seen furthermore in figure 1 the statistics at low Q^2 will be enormous. Therefore we have displayed the expected measurement of $F_2(x,Q^2)$ at lower Q^2 in figure 2b using the parametrization B^- of [7] which has no saturation. As the lines at fixed x indicate, the low x region down to $x = 10^{-4}$ will be explored with high statistics even for luminosities below 10 pb^{-1}. The peculiar hole in the F_2 plot at high energies, figure 2a, results from the low jet energy cut $E_j \geq 5$ GeV^2 [2]. It can be closed, however, running the machine at lower energies. If HERA beam energies will be enlarged after an upgrade and, perhaps, the large luminosities will be reached, the exploration of the high Q^2 region will become very interesting. Figure 2b presents the expectation for F_2 for $\mathcal{L} = 1000\ pb^{-1}$ showing that a precise measurement even up to $Q^2 \simeq 50000$ GeV^2 will be possible.

2.2 $xG_3(x,Q^2)$

The structure function $xG_3(x,Q^2)$

$$xG_3(x,Q^2) = 2x[e_u a_u u_v(x,Q^2) + e_d a_d d_v(x,Q^2)] \tag{6}$$

arises from the γZ interference term. It can be measured from the difference of electron and positron scattering cross sections according to [6]

$$xG_3(x,Q^2) \simeq \left[\frac{d^2\sigma_{nc}^{e^+p}}{dxdQ^2} - \frac{d^2\sigma_{nc}^{e^-p}}{dxdQ^2}\right] \frac{xQ^4}{2\pi\alpha^2}\frac{1}{Y_-\kappa_Z(Q^2)}\frac{1}{2a} \tag{7}$$

where we have neglected the small contribution by $xH_3(x,Q^2)$ [2]. In figure 3 for a luminosity of 1 fb^{-1} (!) a simulated measurement of $xG_3(x,Q^2)$ and of the shape of $xG_3(x)$ averaging over Q^2 are illustrated. Although, the determination of the shape in x could be done with an integrated luminosity of $\mathcal{L} \sim 200\ pb^{-1}$ already, the measurement of the x and Q^2 dependence requires a much higher luminosity because the kinematic factor $Y_- = 1-(1-y)^2$ excludes most of the kinematic range from this measurement as $Y_- \approx 0$ for smaller y values and the $\kappa_Z(Q^2)$ function requires large Q^2 values (≥ 1000 GeV^2). Nevertheless, xG_3 is worth some effort because it allows to directly measure the combination of valence quark distributions $2u_v + d_v$ free of sea quark contaminations down to $x \sim 0.01$. Moreover, at the Born level, the xG_3 term represents the dominant correction in the measurement of F_2 at large y, see eq.2.

2.3 $e^{\pm}d$ scattering

The potential discovery of an unusual cross section behaviour at very low x values will be a major motivation to modify the injection of HERA and, perhaps, accelerate deuterons in the superconducting ring. In ep reactions the charged current structure functions $W_2^{\pm}(x,Q^2)$ and $xW_3^{\pm}(x,Q^2)$ can not be unfolded, since only two cross sections are measured and the flavour-contents of the proton does not allow a separation of the Y_+ and

[2] In this discussion we follow the concept of considering structure functions, independently of their parton model interpretation, as quantities uniquely defined by the invariance properties of the hadronic tensors [9]. In the parton model language one would consider $(\sigma^+ - \sigma^-)\cdot xQ^2/4\pi\alpha^2 Y_-$ as the observable $x\mathcal{F}_3$.

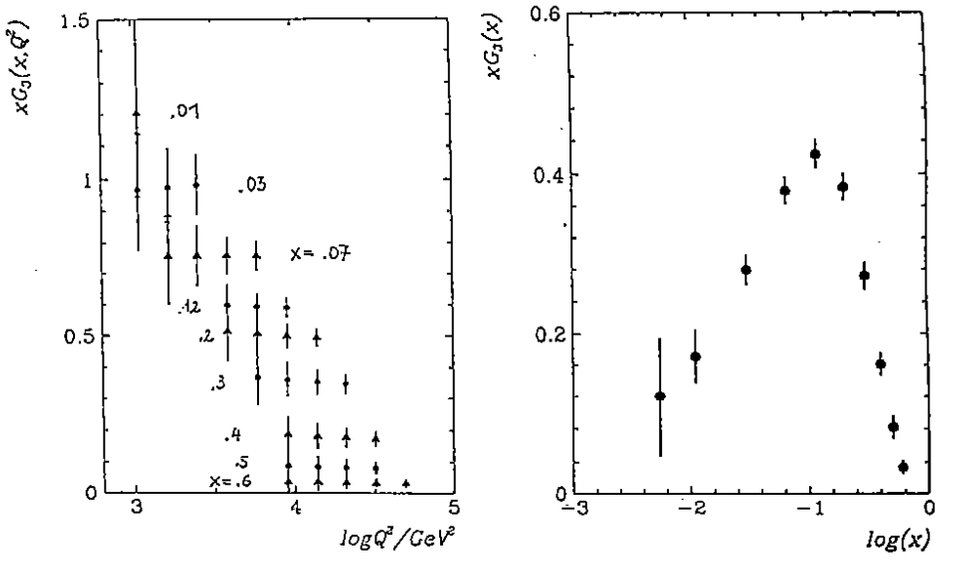

Figure 3: Statistical precision for a measurement of $xG_3(x,Q^2)$ (a) and of $xG_3(x)$ averaged over Q^2 in the accessible kinematical range (b) for $\mathcal{L} = 1\ fb^{-1}$

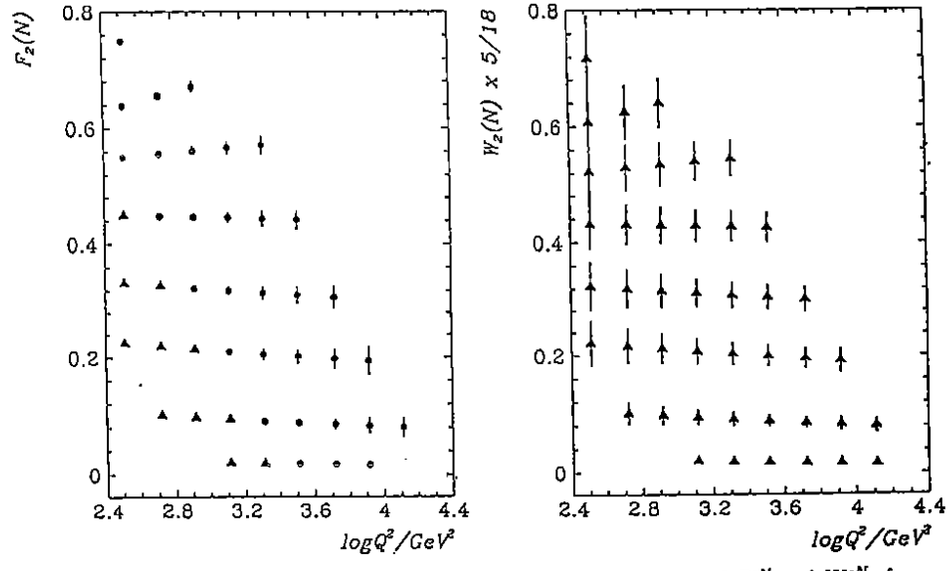

Figure 4: Statistical precision for a measurement with deuterons of F_2^{eN} and W_2^{eN}, for $\mathcal{L} = 100\ pb^{-1}$.

Y_-terms. This is possible, however, in charged current *ed* scattering due to the isospin symmetry of the deuteron:

$$\frac{d^2\sigma^{\pm}}{dxdQ^2} = \frac{2\pi\alpha^2}{x(Q^2+M_W^2)^2}\frac{1}{16\sin^4\theta_W}\left[Y_+W_2^{\pm}(x,Q^2) \mp Y_-xW_3^{\pm}(x,Q^2)\right] \qquad (8)$$

with $W_2^{\pm}(x,Q^2) = \Sigma(x,Q^2)$ and $xW_3^{\pm}(x,Q^2) = x(u_v(x,Q^2)+d_v(x,Q^2)) \pm 2x(s(x,Q^2)+b(x,Q^2)-c(x,Q^2))$. Therefore, the deuteron data will be necessary for the unfolding of quark distributions. Of particular interest is the consideration of neutral *and* charged current cross section data.

Figure4 presents a comparison of the expected high Q^2 measurements of F_2 and W_2 in *ed* sacttering. In the parton model these functions are given by.

$$F_2^{eN}(x,Q^2) = \frac{5}{18}\Sigma(x,Q^2) - \frac{1}{6}x\left[s(x,Q^2)+\bar{s}(x,Q^2)-c(x,Q^2)-\bar{c}(x,Q^2)\right] \qquad (9)$$

and

$$W_2^{eN}(x,Q^2) = W_2^{e^+N}(x,Q^2) = W_2^{e^-N}(x,Q^2) = \Sigma(x,Q^2) \qquad (10)$$

with $N=(p+n)/2$. Note, that the W_2 measurement represents the most precise way of measuring a clean singlet structure function in x and Q^2. In *ep* scattering this could be obtained only from a complicated unfolding procedure [3, 10]

$$\begin{pmatrix} D_1(x,Q^2) \\ D_2(x,Q^2) \\ D_3(x,Q^2) \\ D_4(x,Q^2) \end{pmatrix} = \left(A_{ij}(x,Q^2)\right)\begin{pmatrix} d\sigma_{nc}^+/dxdQ^2 \\ d\sigma_{nc}^-/dxdQ^2 \\ d\sigma_{cc}^+/dxdQ^2 \\ d\sigma_{cc}^-/dxdQ^2 \end{pmatrix} \qquad (11)$$

and less precisely.

It will be interesting to see whether the '5/18 rule' holds at these large Q^2 values. As in neutrino scattering, deviations at small x can be detected and measure the difference of the strange and charm quark distributions [3]

$$x\left[s(x,Q^2)-c(x,Q^2)\right] = 6\left[\frac{5}{18}W_2^{eN}(x,Q^2) - F_2^{eN}(x,Q^2)\right] \qquad (12)$$

Furthermore, from W_2 and xW_3 the sea–quark distribution $\sum x[q_s(x,Q^2)+\bar{q}(x,Q^2)]$ may be derived, see [3].

3 QCD Analysis

As was discussed in [3, 4] already, the structure function $F_2(x,Q^2)$ provides the best possibility among all measurable structure functions at HERA for a QCD test, because it is measurable in a wide (x,Q^2) range with high precision, while in other cases the x shapes of the respective structure functions may be determined [10] only. Being interested here in the expected accuracy of these analyses only, we assume that all relevant corrections have been applied, including e.g. the subleading effects of other structure functions (F_L and xG_3) and the electroweak radiative corrections [11, 5].

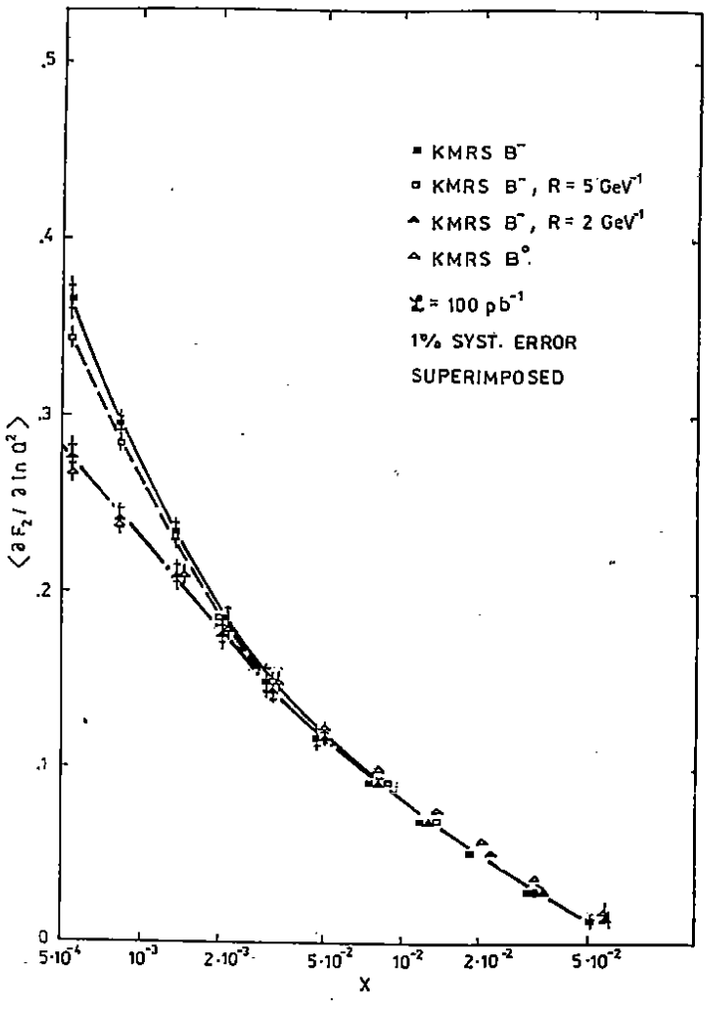

Figure 5: Average slope of F_2, *versus* x using the KMRS parton distributions. The full line corresponds to the B^- set with no screening, the broken line is B^- assuming weak screening ($R = 5$ GeV^{-1}) and the dashed–dotted line B^- with strong screening ($R = 2$ GeV^{-1}). The statistical errors (inner error bars) correspond to $\mathcal{L} = 100\ pb^{-1}$ and $\sqrt{s} = 314$ GeV. A systematical error of 1 % is superimposed.

Approaching the region of small x new dynamical effects may start to influence the evolution of the structure functions [13]. Since the statistics at low x is very high it is important to determine the minimum x down to which these effects may be neglected and the Q^2 evolution be correctly described by the Altarelli–Parisi equations. A convenient way to visualize the strength of new, nonlinear interaction effects [13] will be to consider the quantity $\langle \partial F_2/\partial \ln Q^2 \rangle$. In a first approximation[3] one may use the parametrization of the parton distributions (KMRS, B^-) [7] and compare in the HERA kinematic range the predictions for $F_2(x,Q^2)$ for the case of the Altarelli–Parisi evolution and in the presence of sreening effects ($R = 2\,\mathrm{GeV}^{-1}$). As shown in figure 5 a deviation in $\langle \partial F_2/\partial \ln Q^2 \rangle$ within the experimental errors for $\mathcal{L} = 100\ pb^{-1}$ is not observed up to values of $x_{min} \simeq 2 \cdot 10^{-3}$ which therefore will be taken as the minimum 'allowed' x value.

At lowest possible proton beam energies the acceptance in the valence range $x \geq 0.25$ is large and the statistics, for $\mathcal{L} = 100\ pb^{-1}$, is sufficient to allow for a non–singlet fit using

$$\frac{\partial F_2^{NS}(x,Q^2)}{\partial \ln Q^2} = \frac{\alpha_s(Q^2)}{2\pi}\left\{ x P_{NS}(x) \otimes F_2^{NS}(x,Q^2)\frac{1}{x}\right\} \qquad (13)$$

which yields $\delta\Lambda_{stat} \approx 110$ MeV. In the valence range one may illustrate scaling violations of F_2 by deriving $\langle \partial ln F_2/\partial ln Q^2 \rangle$ directly from the data. As becomes clear from eq.13 this quantity is directly proportional to α_s and the remaining factor depends only weakly on Q^2. The measurement of this quantity at HERA will require to run at low E_p [2], to collect high luminosity and to understand the region of very low scattering angle. Figure 5b shows the statistical error of Λ as a function of the minimum scattering angle in the valence range. One sees that roughly each degree lost worsens $\delta\Lambda_{stat}$ by ~ 80 MeV.

The measurement of the scaling violations of $F_2(x,Q^2)$ in the x range $x \geq x_{min}$ requires to determine Λ in a combined fit together with the initial distributions $\Sigma(x,Q_0^2) = \sum_{i=1}^{N_f} x(q_i(x,Q_0^2) + \bar{q}_i(x,Q_0^2))$, the nonsinglet function $\Delta(x,Q_0^2) = \sum_{i=1}^{N_f/2} x\left[u_j(x,Q_0^2) + \bar{u}_j(x,Q_0^2) - d_j(x,Q_0^2) - \bar{d}_j(x,Q_0^2)\right]$ and the gluon distribution $xG(x,Q_0^2)$ using the evolution equations:

$$\begin{aligned}
\frac{\partial F_2(x,Q^2)}{\partial \ln Q^2} &= \frac{\alpha_s(Q^2)}{2\pi} x\left\{\frac{1}{6} P_{NS}(x) \otimes \Delta(x,Q^2)\frac{1}{x}\right\} \\
&+ \frac{\alpha_s(Q^2)}{2\pi} x\left\{\frac{5}{18}\left[P_{ff}(x) \otimes \Sigma(x,Q^2)\frac{1}{x} + 2N_f P_{fg}(x) \otimes G(x,Q^2)\right]\right\} \\
\frac{\partial G(x,Q^2)}{\partial \ln Q^2} &= \frac{\alpha_s(Q^2)}{2\pi}\left\{P_{gf}(x) \otimes \Sigma(x,Q^2)\frac{1}{x} + P_{gg}(x) \otimes G(x,Q^2)\right\} \qquad (14)
\end{aligned}$$

which are given in leading order here.

To use the maximum accessible range in x and Q^2 (see [2]) we combine the data sets at $s_1 = 4 \cdot 10 \cdot 300$ GeV^2 and $s_2 = 4 \cdot 30 \cdot 820$ GeV^2 with $\mathcal{L} = 100\ pb^{-1}$ for each cms energy requiring $Q^2 > 10\,\mathrm{GeV}^2$. In figure 6c,d the dependence of the resulting statistical error of Λ on the minimum value of Q^2 and x are shown. In the analysis we applied the algorithms [15]. For the range $x \geq 2 \cdot 10^{-3}$ and $Q^2 > 10\,\mathrm{GeV}^2$ one obtains $\delta\Lambda_{stat} \approx 50$ MeV. One may need to cut at $x > 10^{-2}$ which still yields $\delta\Lambda_{stat} \approx 100$ MeV.

If one restricts the full fit to the range $x \leq 0.25$ the resulting measurement may be compared with the pure valence region result. Figure 7 displays the two corresponding

[3] See [14] for a description of F_2 and F_L referring to an appropriate factorization scheme.

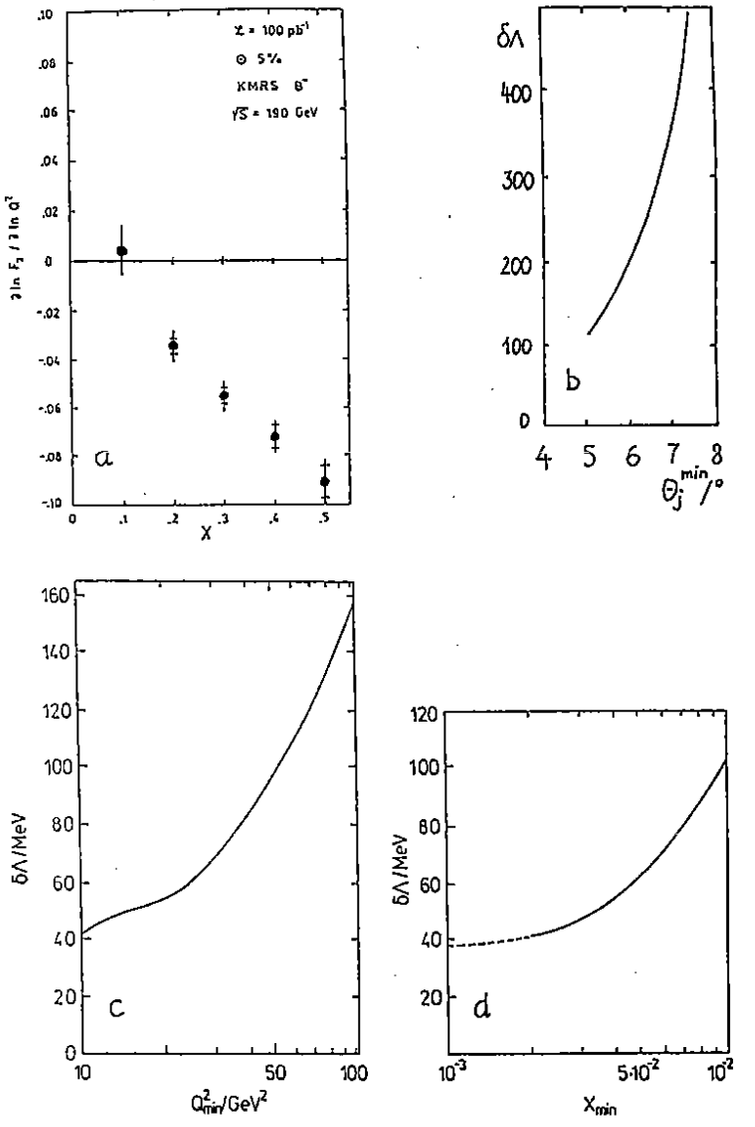

Figure 6: (a) Average slope $\langle \partial F_2/\partial \ln Q^2 \rangle$ *versus* x using the KMRS distribution B^- in the valence range. The inner error bars represent the statistical error for 100 pb^{-1} with a systematical error of 5% superimposed. (b) Dependence of $\delta\Lambda_{stat}$ for $x \geq 0.25$ 100 pb^{-1} and $\sqrt{s} = 110$ GeV on the minimum jet angle. Dependence of $\delta\Lambda_{stat}$ on the minimum Q^2 (c) and x (d) used in the QCD fit for the combined data sets at $\sqrt{s} = 110$ and 314 GeV for $\mathcal{L} = 100\ pb^{-1}$ each.

values of α_s which are statistically distinct at the level of two standard deviations for 100 pb^{-1}.

The slope of F_2 for $x \lesssim 0.1$ is dominated by the contribution due to the gluon distribution [4]. Therefore a QCD analysis in this range may be performed by fixing the parameters of the quark distributions at Q_0^2 and fitting Λ together with the parameters of the initial gluon distribution. One may assume different shapes of $xG(x,Q_0^2)$, e.g.

$$xG(x,Q_0^2) = A \cdot x^{\alpha} \cdot (1-x)^{\beta} \tag{15}$$

with $\int_0^1 xG(x,Q_0^2)\,dx = 1/2$. This leaves Λ and two further parameters for this particular fit. As two extreme cases we consider $\alpha = 0$ and $\alpha = -1/2$ setting $\beta = 5$. Restricting the analysis to the kinematical region $x \in [0.002, 0.1]$ and combining the two data samples at low and high $\sqrt{s}$ we obtain parameter ranges which can be used to draw corresponding error bands for $xG(x,Q_0^2)$, see figure 8. In particular, for the exponent α we obtain a statistical error of $\pm$ 0.05 for 100 pb^{-1}.

4 Conclusions

The structure function $F_2^{ep}(x,Q^2)$ can be measured from very small values of $x \sim 10^{-4}$ and up to high values of $Q^2 \sim \mathcal{O}(10^4\,\mathrm{GeV}^2)$. For this measurement a detailed understanding of the electroweak radiative corrections, the contributions due to $F_L(x,Q^2)$ and due to $xG_3(x,Q^2)$ to $d\sigma^{e^{\pm}p}/dxdQ^2$ is needed. A complete analysis, even of F_2 only, requires to run HERA also at lower cms energies and to measure both $d\sigma^{e^+p}/dxdQ^2$ and $d\sigma^{e^-p}/dxdQ^2$.

In the case of neutral current scattering one may use different methods to determine the kinematical variables, i.e. the electron measurement, the measurement of the current jet, use the so called mixed variables (Q_e^2, y_J) or others. Thus different possibilities exist to cross control and to determine the values of x and Q^2 for the cross section measurements.

At $\mathcal{L} = 200\ pb^{-1}$ the structure function $(xG_3(x,Q^2))_{Q^2}$ may be measured at a precision for which its shape in x can be determined. Being a nonsinglet function it gets weakly modified by the evolution in Q^2 only. If a measurement is intended of $xG_3(x,Q^2)$ also *versus* Q^2, an integrated luminosity of $\mathcal{L} \simeq 1\,fb^{-1}$ is required.

Different methods exist to determine parton distributions for individual flavours or combinations of them. These methods ar either based on direct linear unfoldings from the measurements of the four differential cross sections $d\sigma^{e^{\pm}p}_{nc,cc}/dxdQ^2$ or approximative representations in certain ranges of x and Q^2 [3, 10]. For various distributions, however, the use of deuterons instead of protons will provide superior and complementary information on the parton distributions.

After an upgrade of HERA electron and proton beam energies of $E_e = 45$ GeV and $E_p = 1140$ GeV might be reached, corresponding to $\sqrt{s} = 453$ GeV. However, detailed investigations of the very high Q^2 region will be possible only if an integrated luminosity of $\mathcal{L} \sim 1\ fb^{-1}$ can be achieved.

The measurement of Λ and $\alpha_s(Q^2)$ from the scaling violations of structure functions will be based on the measurement of $F_2(x,Q^2)$. A nonsinglet analysis appears to be feasible but relies dominantly on low s data *and* on a good measurement of the hadron flow down to $\theta_J \sim 5°$. Then for $\mathcal{L} = 100\ pb^{-1}$ and $\sqrt{s} = 110\,\mathrm{GeV}$ one obtains $\delta\Lambda_{stat} = 110\,\mathrm{MeV}$ in a nonsinglet analysis. From a full analysis combining two data sets at low and high

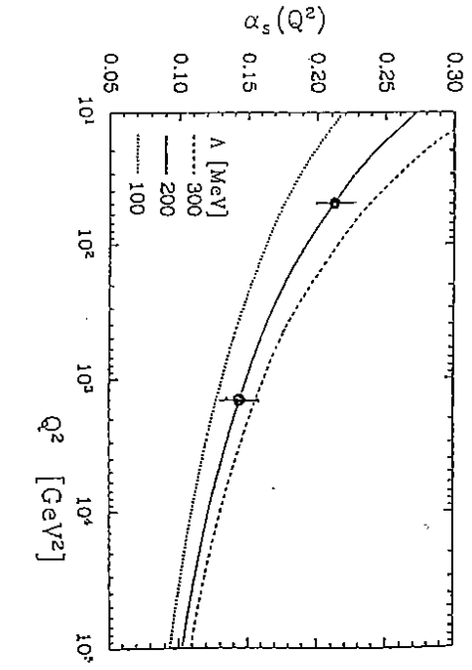

Figure 7: Dependence of α_s on Q^2 from a combined fit using two samples of $\sqrt{s} = 314\,\mathrm{GeV}$ and $\sqrt{s} = 110\,\mathrm{GeV}$ with $\mathcal{L} = 100\ pb^{-1}$ each. The upper point corresponds to a nonsinglet fit for $\theta_J > 5°$ and $x > 0.25$. The lower point at $Q^2 \sim 50\,\mathrm{GeV}^2$ corresponds to a fit in the range $x < 0.25$.

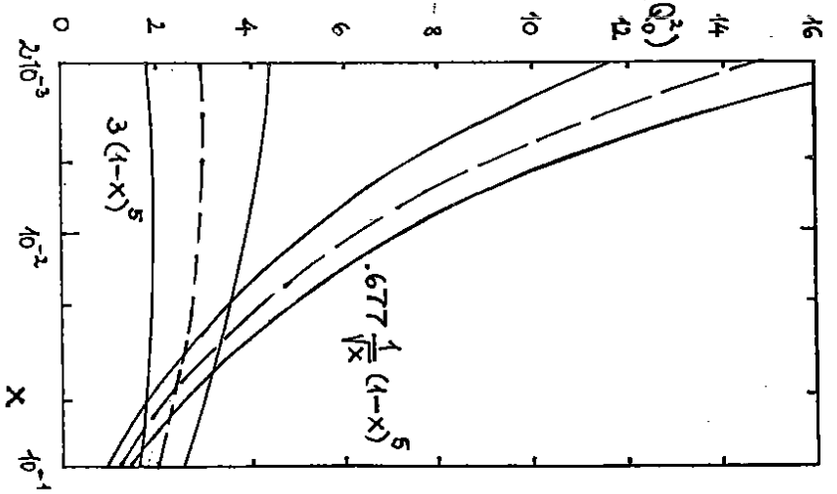

Figure 8: Possible determination of $xG(x,Q_0^2)$ in a QCD fit for $x < 0.1$, see text. The upper error band corresponds to the choice $\alpha = -0.5$ and the lower band to $\alpha = 0$, see eq. 15. The inner error denotes the statistical error for $\mathcal{L} = 100\ pb^{-1}$ for both the low and high s option.

energies one can expect an error of about 50 MeV for the same luminosities. Comparing the measurements of α_s in the ranges $x \leq 0.25$ and $x \geq 0.25$ its Q^2 dependence may be statistically established.

A dedicated analysis of the shape of the gluon distribution should lead to the determination of the leading power α to an accuracy of about $\pm$ 0.05.

References

[1] S.Bentvelsen, J.Engelen and P.Kooijman , these proceedings;
G.Bernardi and W.Hildesheim, these proceedings

[2] M.Klein , these proceedings

[3] J. Blümlein, M. Klein, T. Naumann and T. Riemann, Proc. of the 1987 HERA Workshop, ed. R.D. Peccei, (DESY, Hamburg, 1988), p. 67.;
J. Blümlein, M. Klein and T. Naumann, Proc. 'New theories in physics', Kazimierz, Poland, eds. Z. Ajduk et al., (World Scientific, Singapore, 1989), p. 228.

[4] J. Blümlein, G. Ingelman, M. Klein and R. Rückl, Z. Phys. **C45** 501 (1990).

[5] For a recent survey see: H. Spiesberger, A. Akhundov, A. Anlauf et al., these proceedings, Vol.I and references given there.

[6] M.Klein and T.Riemann, Z. Phys. **C24** 151 (1984).

[7] J.Kwiecinski, A.D. Martin, W.J. Stirling and R.G. Roberts, Phys. Rev. **D42** 798 (1990).

[8] J. Blümlein and M. Klein, in preparation.

[9] E.Derman, Phys. Rev. **D7** 2755 (1973).

[10] G. Ingelman and R. Rückl, Z. Phys. **C44** 291 (1989).

[11] D.Y. Bardin, C. Burdik, P.C. Christova and T. Riemann, Z. Phys. **C42** 679 (1989);
J. Blümlein, Z. Phys. **C47** 89 (1990);
H. Spiesberger, DESY 89–175;
J. Blümlein, Phys. Lett. **B271** 267 (1991).

[12] A. Cooper Sarkar, R.C.Devenish and M.Lancaster OUNP-91-35 and these proceedings.

[13] L.V. Gribov, E.M. Levin and M.G. Ryskin, Phys. Rep. **100** 1 (1983); J. Collins and J. Kwiecinski, Nucl. Phys. **B335** 89 (1990); J. Bartels, J. Blümlein and G. Schuler, Nucl. Phys. B (Proc. Suppl.) **18C** 147 (1990) and Z. Phys. **C50** 91 (1991).

[14] J. Blümlein, in preparation.

[15] W. Furmanski and R. Petronzio, Nucl. Phys. **B195** 237 (1982);
L.F. Abbott, W.B. Atwood and R.M. Barnett, Phys. Rev. **D22** 582 (1980) .